



HAL
open science

Strong temporal and spatial variation of dissolved Cu isotope composition in acid mine drainage under contrasted hydrological conditions

J. Masbou, Jérôme Viers, Jose Antonio Grande, R. Freydier, Cyril Zouiten, Patrick Seyler, O.S. S Pokrovsky, Philippe Behra, Brigitte Dubreuil, M.L. de La Torre

► To cite this version:

J. Masbou, Jérôme Viers, Jose Antonio Grande, R. Freydier, Cyril Zouiten, et al.. Strong temporal and spatial variation of dissolved Cu isotope composition in acid mine drainage under contrasted hydrological conditions. *Environmental Pollution*, 2020, 266 (Part 2), 10.1016/j.envpol.2020.115104 . hal-02899647

HAL Id: hal-02899647

<https://hal.inrae.fr/hal-02899647v1>

Submitted on 18 Jul 2022

HAL is a multi-disciplinary open access archive for the deposit and dissemination of scientific research documents, whether they are published or not. The documents may come from teaching and research institutions in France or abroad, or from public or private research centers.

L'archive ouverte pluridisciplinaire **HAL**, est destinée au dépôt et à la diffusion de documents scientifiques de niveau recherche, publiés ou non, émanant des établissements d'enseignement et de recherche français ou étrangers, des laboratoires publics ou privés.



Distributed under a Creative Commons Attribution - NonCommercial 4.0 International License

1 Strong temporal and spatial variation of dissolved Cu isotope 2 composition in acid mine drainage under contrasted hydrological 3 conditions 4

5 Masbou^{1,2} J., Viers^{1*} J., Grande³ J-A., Freydier⁴ R., Zouiten¹ C., Seyler⁴ P., Pokrovsky^{1,5} O.,
6 Behra⁶ P., Dubreuil⁶ B., de la Torre³ M-L.

7
8 1 : Géosciences Environnement Toulouse (GET), Université de Toulouse, CNRS, IRD 14
9 avenue Edouard Belin, 31400 Toulouse, France

10 2 : Laboratoire d'Hydrologie et de Géo chimie de Strasbourg (LHyGeS), Université de
11 Strasbourg/ENGEEES, CNRS, 1 rue Blessig, 67084, Strasbourg Cedex, France

12 3 : Centro de Investigación para la Ingeniería en Minería Sostenible, Escuela Técnica
13 Superior de Ingeniería, Universidad de Huelva, Ctra. Palos de la Frontera, s/n, 21819 Palos de
14 la Frontera, Huelva, Spain

15 4 : Laboratoire HydroSciences UMR 5569, CNRS, IRD, Université de Montpellier, 163 Rue
16 Auguste Broussonnet, CC 57, 34090, Montpellier, France

17 5 : BIO-GEO-CLIM Laboratory, Tomsk State University, 36 Lenina Prs, Tomsk, Russia

18 6 : Laboratoire de Chimie Agro-industrielle, LCA, Université de Toulouse, INRA, Toulouse,
19 France

20
21 * Corresponding author: Jérôme Viers, Ph.D.

22

23

24 **Abstract**

25 Copper export and mobility in acid mine drainage are difficult to understand with
26 conventional approaches. Within this context, Cu isotopes could be a powerful tool and here
27 we have examined the relative abundance of dissolved ($< 0.22 \mu\text{m}$) Cu isotopes ($\delta^{65}\text{Cu}$) in the
28 Meca River which is an outlet of the Tharsis mine, one of the largest abandoned mines of the
29 Iberian Pyrite Belt, Spain. We followed the chemical and isotopic composition of the
30 upstream and downstream points of the catchment during a 24-h diel cycle. Additional $\delta^{65}\text{Cu}$
31 values were obtained from the tributary stream, suspended matter ($> 0.22 \mu\text{m}$) and bed
32 sediments samples. Our goals were to 1) assess Cu sources variability at the upstream point
33 under contrasted hydrological conditions and 2) investigate the conservative vs. non
34 conservative Cu behavior along a stream. Average $\delta^{65}\text{Cu}$ values varied from -0.47 to -0.08 ‰
35 ($n=9$) upstream and from -0.63 to -0.31‰ downstream ($n=7$) demonstrating that Cu isotopes
36 are heterogeneous over the diel cycle and along the Meca River. During dry conditions, at the
37 upstream point of the Meca River the Cu isotopic composition was heavier which is in
38 agreement with the preferential release of heavy isotopes during the oxidative dissolution of

39 primary sulfides. The more negative values obtained during high water flow are explained by
40 the contribution of soil and waste deposit weathering. Finally, a comparison of upstream vs.
41 downstream Cu isotope composition is consistent with a conservative behavior of Cu, and
42 isotope mass balance calculations estimate that 87 % of dissolved Cu detected downstream
43 originate from the Tharsis mine outlet. These interpretations were supported by
44 thermodynamic modelling and sediment characterisation data (X-ray diffraction, Raman
45 Spectroscopy). Overall, based on contrasted hydrological conditions (dry vs flooded), and
46 taking the advantage of isotope insensitivity to dilution, the present work demonstrates the
47 efficiency of using the Cu isotopes approach for tracing sources and processes in the AMD
48 regions.

49
50 **Keywords:** copper; isotopes, Acid Mine Drainage (AMD); river; flood

51

52 **1. Introduction**

53 The Iberian Pyrite Belt (South-west Spain), which is among the largest metallogenic
54 provinces in the world, presents serious problems of Acid Mine Drainage (AMD) (Almodovar
55 et al., 1997; Leblanc et al., 2000 ; Grande et al., 2010, 2013; Olias et al., 2019) due to the
56 intense mining activity that occurred during different periods of history including the present
57 time. In particular, during the most active period, from the mid-XIXth to the XXth centuries,
58 large amounts of abandoned waste have been left over the whole region (Pérez Ostalé, 2014).
59 Induced AMD phenomenon leads to surface waters with low pH, and a high metal and
60 sulphate load that strongly affect both inland and marine ecosystems since the two largest
61 AMD affected watersheds of the region, the Odiel and Tinto Rivers, deliver their waters to the
62 estuary of Huelva (Achterberg et al., 2003; Sainz et al., 2004; Nieto et al., 2007; Grande et al.,
63 2018). Due to scarcity of water in this region of the South-West of Europe, the AMD can
64 strongly impact the aquatic ecosystems and surface and groundwater quality (see

65 www.fao.org). Despite the numerous studies dealing with the AMD processes origins and
66 consequences on waters, soils and biota (e.g., Elbaz-Poulichet et al., 2001) the metal
67 distribution, reactivity and transport mechanisms in the rivers still remain poorly known.

68 In addition to dissolved and particulate metals concentrations monitoring in surface waters,
69 the stable isotopes of metals (Cu, Fe, Zn...) are now routinely used to trace the source of
70 metals in the environment and to reveal the biotic and abiotic mechanisms controlling
71 elements transfer within a watershed (see Teng et al. (2017) for a review). As most of the
72 mines in the Iberian Pyrite Belt were mined for copper (Saez et al., 1999), we looked at the
73 potential contribution of copper isotopes to better understand this metal behaviour in such
74 areas. A number of works addressed Cu isotopes in the AMD context (Mathur et al., 2005;
75 Balistrieri et al., 2008; Borrok et al., 2008; Fernandez and Borrok, 2009; Kimball et al., 2009;
76 Mathur et al., 2009; Pérez Rodríguez et al., 2013; Mathur et al., 2014; Song et al., 2016;
77 Dótor-Almazán et al., 2017; Viers et al., 2018; Roebbert et al., 2018). Carried out during
78 steady hydrological conditions, these studies showed that sulfide mineral dissolution in
79 oxygenic conditions essentially controls the Cu isotopes distribution in surface and ground
80 waters. Extensive natural observations and experimental works evidenced strong enrichment
81 in heavy Cu isotopes of aqueous solution interacting with primary sulfide minerals. Moreover,
82 in contrast to relatively narrow range of isotopic signature ($\delta^{65}\text{Cu}$) in these primary minerals,
83 the secondary mineral products exhibit a $\delta^{65}\text{Cu}$ variability as high as from -17 to +10 ‰, see
84 (Mathur et al., 2009). The speciation of Cu in sulfide mine environments is extremely
85 complex because Cu is present in numerous secondary minerals whose proportions strongly
86 depend on the hydrological regime (wetting and drying) (Valente et al., 2013). Moreover, the
87 formation of these minerals in mine-impacted surface waters is controlled by key parameters
88 such as pH, temperature, redox conditions, saturation state and biological activity (Sanchez-
89 Espana et al., 2005, 2011; Sarmiento et al., 2009a,b). High sensitivity to fractionation of

90 copper isotopes in supergene environments makes copper isotopes a good potential tracer for
91 metal transfer within the continuum mine – river – lake encountered in the Iberian Pyrite Belt.

92 To better understand the environmental factors controlling Cu concentration and isotopes
93 fractionation in AMD aquatic settings, our initial objective was to study the evolution of
94 chemical and isotopic fractionation during a diel cycle (24h) in an AMD impacted river.
95 Indeed, several parameters and processes that are often interrelated (T° , dissolved O_2 , water
96 discharge, pH...) may influence the concentration of the chemical species during a diel cycle
97 in the water (Nimick et al., 2011). To address this issue within the AMD context, we used a
98 representative scenario of strongly contaminated Meca River (Huelva, SW Spain) of the
99 Iberian Pyrite Belt. This river drains the abandoned copper mine of Tharsis - one of the
100 largest in the area - and delivers its waters to the Sancho Lake. Taking the advantage of an
101 extremely strong rainy event that occurred during the sampling period, we primarily focused
102 on studying the response of a mining system to variable hydrological stage. Further, in order
103 to quantify the spatial variability of Cu isotope composition in the AMD-affected Meca River,
104 we performed measurements in two points, one at the outlet of the mining district and one 20
105 km downstream, three hours each during 24 hours. We expected that by examining the
106 variation of Cu isotopic composition in time and space, we can better understand the transfer
107 and origin of Cu and other metals within the mining area and reveal the mechanisms of Cu
108 isotopes fractionation in these environmentally important riverine systems.

109

110 **2. Site description**

111 *2.1. Geology of the Iberian Pyrite Belt*

112 The study area belongs to the Iberian Pyrite Belt (IPB), located in the south-west of the
113 Iberian Peninsula. This IPB is approximately 240 km long and 50 km wide and is one of the

114 largest stocks of massive sulfides of volcanogenic origin in the world. It includes more than
115 90 mines (Saez et al., 1999). Pyrite (FeS_2) is the main ore mineral but one finds a procession
116 of other metallic sulfides such as sphalerite (ZnS), galena (PbS), chalcopyrite (CuFeS_2),
117 arsenopyrite (FeAsS) and there is a large variety of other metal sulfides containing minor
118 quantities of Cd, Sn, Ag, Au, Co, Hg. Today, the majority of these mines are abandoned even
119 though some remain in operation. Details about the geology of this area can be found in
120 Tornos et al. (2008) and Conde et al. (2009).

121

122 *2.2. Hydroclimatic conditions*

123 The study area, located in the Huelva province, has a Mediterranean climate, which can be
124 classified as semi-arid. Annual precipitation is about 630 mm/year, being mostly concentrated
125 in the wet season from October to May, and the average annual temperature is 17.1 °C
126 (<http://www.aemet.es>).

127 Our study took place in the watershed of the Meca River, a tributary of the Odiel River.
128 The Odiel River joins the Tinto River at the city of Huelva. The average water discharge of
129 the Odiel River is around $10 \text{ m}^3 \cdot \text{s}^{-1}$ at Gibraleon, a town close to the river mouth (see
130 ConfederacionHidrografica del Guadiana; <https://www.chguadiana.es>). The Odiel watershed
131 with a surface of 2300 km^2 and a length of 140 km accounts for about 80% of the continental
132 water reaching the estuary of Huelva (Santisteban, 2015). The whole river network is
133 impacted by acid mine drainage (Grande et al., 2018). This is especially correct for the Meca
134 River due to the presence of the Tharsis mine, in the upstream part of its catchment. Although
135 it is now abandoned, Tharsis is one of the largest mining districts with almost 100 Mt of
136 estimated resources (Conde et al., 2009). Further details of the Tharsis mine can be found in
137 Perez Ostale (2014) and Valente et al. (2013).

138 The weather was particularly rainy during the field sampling (11 to 12-May-2016). It
139 rained 58 mm the preceding three days (8 to 10-May-2016) to our sampling (Alosno station)
140 and 24 mm on the 11-May-2016. Unfortunately, we do not have the whole dataset for rain
141 water because the weather station was destroyed during this storm event; As the Meca River
142 water discharge is not monitored continuously, we performed a measurement of the water
143 discharge using the “bucket method” when it was possible. Using previous work done by
144 Galvan et al. (2009) within the Meca River catchment, sulphate concentrations could be used
145 in the first order to account for the relative variation in water discharge. Indeed, these authors
146 proposed the following relation between sulphate concentration (SO_4) and water discharge
147 (Q) : ($[SO_4] = 362.1 * Q^{-0.30}$). No relation was proposed by these authors between Cu
148 concentration and Q due to the lack of reproducibility.

149

150 **3. Materials and methods**

151 *3.1. Sampling protocol*

152 Sampling strategy aimed to study the geochemical processes along the Meca River during
153 a complete diel cycle (24 h). Geographical gradient was investigated by collecting water
154 samples simultaneously by two different teams in two sampling sites (Fig. 1): *i*) the Tharsis
155 Mine outlet located upstream of the watershed called ‘upstream’ and *ii*) a point located 20 km
156 downstream (called ‘downstream’). Sampling was achieved in a similar timeframe of 24h for
157 the two sites, between 11-May-2016 4:00 p.m. and 12-May-2016 5:00 p.m. with a time step
158 of 3 hours. In addition, one sample of the main Meca tributary (between the two points) was
159 also collected (Tributary stream, Fig. 1). In addition to water samples, a bedload sediment
160 sample from the Meca River was collected at the upstream point.

161 At each sampling point, the values of pH, dissolved O₂, temperature, and specific
162 conductivity were measured *in-situ* using a portable multi-parameter instrument (WTW®,
163 340i). Protocols for the measurement of these parameters and the sampling method are
164 reported in Viers et al. (2018). Among the collected samples, the 0.22 µm membrane of four
165 selected samples were conserved to recover suspended sediments and perform chemical
166 analyses. In addition to 0.22 µm filtration, an ultrafiltration at 1,000 Da were carried out on
167 four selected samples collected upstream (11-May-2016 4:00 p.m., 11-May-2016 10:00 p.m.,
168 12-May-2016 4:00 a.m., 12-May-2016 10:00 a.m.) using a 50 mL Amicon® ultrafiltration
169 cell. Details of ultrafiltration procedure, analyses of possible artifacts and yields are given
170 elsewhere (Viers et al., 1997; Dupré et al., 1999; Vasyukova et al., 2010).

171

172 *3.2. Mineralogical characterization*

173 Two suspended sediments collected at the upstream point (ME-A 11-May-2016 10 p.m.
174 and ME-A 12-May-2016 4 p.m. samples) were characterised by SEM-EDX (form, chemical
175 composition) at the Centre de MicroCaractérisation Raimond Castaing (Toulouse) and by X-
176 Ray Diffraction at the GET laboratory (Toulouse). All the details about the methods are
177 reported in Blondet et al. (2019) and Blotevogel et al. (2018).

178 The Raman spectra of the ME-A 11-May-2016 10 p.m. sample was obtained at room
179 temperature by the confocal microscope Raman spectrometer (Horiba Scientific Labram HR
180 evolution spectrometer) equipped with charge coupled device (CCD) as detector at the LCA
181 laboratory of the Ensiacet (INPT). We used the 532 nm laser as excitation source and a dry
182 objective MPLN x100 (NA: 0.90 µm). Measurement conditions were: laser power of 2.5 mW
183 during 1 second and 2 accumulations; pinhole: 100 µm; spectral range: 100 to 2400 cm⁻¹
184 scanned with a high-resolution grating with 1800 gr/mm; Raman spectra: recorded directly

185 from powder. Raman spectral libraries from Bio-Rad and KnowItAll® ID Expert™
186 spectroscopy software were used for the identification.

187

188 *3.3. Elemental content determination (major and Trace Elements (TE))*

189 Major and trace element concentrations were measured using ICP-MS (iCAP Q, Thermo
190 Scientific- Kinetic Energy Discrimination mode using He) at the AETE-ISO platform (OSU
191 OREME/Université de Montpellier). Concentrations were determined with external
192 calibration using (Be, Sc, Ge, Rh, Ir) as internal standards to correct potential sensitivity
193 drifts. The quality of the analysis was checked by analyzing international certified reference
194 waters (CNRC SLRS-6). The accuracy was better than 5% relative to the certified values and
195 the analytical error (relative standard deviation) was better than 5% for concentrations ten
196 times higher than the detection limits. Anions concentrations were determined by ionic
197 chromatography at the GET laboratory.

198 In addition to total measurements, Fe speciation (Fe^{2+} and Fe^{3+}) was determined by
199 spectrophotometry and on-site using ferrozine method (Viollier et al., 2000). These
200 measurements were performed on the dissolved fraction ($<0.22 \mu\text{m}$) immediately after
201 sampling for the upstream samples.

202 Before analysis, sediments were digested at the GET laboratory. For each sample, 100 mg
203 of sediment were precisely weighed in Teflon vessels. 1 mL of H_2O_2 and 0.5 mL of bidistilled
204 HNO_3 were added to the samples and left at room temperature for 24 hours. Then, 1 mL of
205 HNO_3 is added and the solutions were warmed at 80°C for 24 h. The solution is then
206 evaporated on a plate at 80°C . 1.2 ml of HF and 1.2 ml of bidistilled HNO_3 are then added for
207 a new warming step at 80°C . After evaporation, 20 drops of bidistilled HCL and 10 drops of
208 bidistilled HNO_3 are added. The acid solution was warmed at 115°C for 24 h and finally

209 evaporated at 80°C. After complete evaporation, the remaining solid residue for each sample
210 was dissolved in 10 mL of a 10% HNO₃ solution. Acid blanks and certified reference material
211 samples (LKSD-03, lake sediment samples) were also used to ensure the quality of the
212 measures and their traceability.

213

214 *3.4. Cu isotopes determination*

215 Water sample aliquots containing approximately 1000 ng of Cu were purified using anion
216 exchange chromatography on AG-MP1 resin (BIORAD) following an adapted protocol from
217 Borrok et al. (2008). The protocol was repeated twice in order to ensure a complete separation
218 of Cu from the matrix. The total procedure blank was negligible in comparison with the
219 amount of Cu in the samples (<1%). Column yields and remaining elements such as (Na, Mg,
220 Ca, Ti, Cr) that can interfere with Cu and Zn isotopes (Petit et al., 2008) were checked for
221 each samples using Q-ICP-MS iCAP Q (Thermo Scientific). The yield was 100 ± 5% and no
222 interfering elements were found in the solutions. Cu isotopic analyses were performed on a
223 multiple-collector inductively coupled plasma mass spectrometer (MC-ICP-MS) Neptune
224 Plus (Thermo Scientific®), using SIS (Stable introduction System) nebulization chamber and
225 PFA self-aspiration nebulizer (50 µl.min⁻¹, Elemental Scientific®) at Plateforme AETE-ISO
226 (OSU OREME-Université de Montpellier, France). Each sample was analyzed three times
227 and was bracketed with the SRM NIST 976 copper solution. Cu isotopes (⁶³Cu, ⁶⁵Cu), Zn
228 isotopes (⁶⁴Zn, ⁶⁶Zn, ⁶⁷Zn, ⁶⁸Zn), and Ni isotope (⁶²Ni) were monitored simultaneously.
229 Measurements of ⁶²Ni signal allowed correcting the possible isobaric interference of ⁶⁴Ni on
230 ⁶⁴Zn. A Zn solution JMC 3e0749-L from Lyon was added to the samples in order to correct
231 instrumental mass bias using the ⁶⁶Zn/⁶⁴Zn ratio (exponential law) and the method of sample-
232 standard bracketing was used to determine the δ⁶⁵Cu (Marechal et al., 1999). The 2σ variation
233 obtained on the 3 independent δ⁶⁵Cu measurements was 0.01-0.06 ‰.

234 $\delta^{65}\text{Cu}$ (in units of ‰) is the Cu isotopic deviation relative to a standard, the SRM NIST-
235 976:

$$236 \quad \delta^{65}\text{Cu} = \left(\left(\frac{\left(\frac{{}^{65}\text{Cu}}{{}^{63}\text{Cu}} \right)_{\text{sample}}}{\left(\frac{{}^{65}\text{Cu}}{{}^{63}\text{Cu}} \right)_{\text{NIST976}}} \right) - 1 \right) \times 1000$$

237

238 2.3. Thermodynamic calculations

239 Thermodynamic analysis including calculations of the speciation and the saturation
240 indexes have been performed for the Meca River (upstream and downstream points) with
241 respect to the common minerals of mining environments and specifically those described for
242 the Tharsis mine by previous studies (Sanchez-Espana et al., 2005; Valente et al., 2013).
243 Following these studies, we considered that goethite, ferrihydrite, jarosite, gibbsite,
244 schwertmannite, (hydro)basaluminite, and gypsum may precipitate from aqueous solution.
245 Modelling calculations were done using Visual MINTEQ ver. 3.0. In the case of the minerals
246 schwertmannite and hydrobasaluminite the solubility product constants ($\log K_{\text{sp}}$) were taken
247 from Sanchez-Espana et al. (2011) and the calculations were done manually using the element
248 activities given by Visual Minteq 3.0. It is visible that their value for schwertmannite ($\log K_{\text{sp}}$
249 = 18.8 ± 3.5 ; pH range = 2.6 – 5.2) is very similar to that proposed by Bigham et al. (1996)
250 ($\log K_{\text{sp}} = 18.0 \pm 2.5$; pH range = 2.8 – 3.2). The results of speciation and saturation indexes
251 are reported in the supplementary information (Table S1 A and B).

252

253 3. Results

254 *3.1. Variation of the water conductivity and pH in the Meca River*

255 In the upstream point, conductivity varies from 2.8 to 11.4 mS/cm and pH varies between
256 2.43 and 2.82 (Table 1). At the downstream point, conductivity is much lower (from 0.31 to
257 0.54 mS/cm) and pH is higher with values ranging between 3.61 and 5.68. The Meca tributary
258 exhibits intermediate values with a pH of 3.85 and a conductivity of 0.51 mS/cm.

259 Element concentrations in the river water are reported in Table 1. At the upstream point,
260 the anionic load is dominated by SO_4^{2-} (> 99%) and the cationic load is dominated by Fe (>
261 50%), Mg^{2+} (> 20%), Al^{3+} (> 15%), Zn^{2+} and Ca^{2+} (> 4%) and Cu^{2+} (~1%). At the
262 downstream point, the anionic load is dominated by SO_4^{2-} (> 60%) and Cl^- (> 30%) while the
263 cationic load is dominated by Mg^{2+} (> 35%), Na^+ (> 30%), Ca^{2+} (> 20%), and Fe (> 6%).
264 Copper accounts for less than 0.5% of the cationic load at the downstream point. In the Meca
265 tributary, the anionic load is dominated by SO_4^{2-} (70%), followed by Cl^- and NO_3^- (15%). The
266 cationic load is dominated by Mg^{2+} (40%), Ca^{2+} (30%) and Na^+ (20%). Elemental
267 concentrations are generally much lower in the downstream sampling point (e.g., 80 times for
268 Cu) because of dilution process. However, we note that Cl, NO_3^- and K concentrations are
269 higher in the downstream sampling point while Na concentration is rather similar in the two
270 sampling points.

271

272 *3.2. Copper concentration and isotope composition of Meca River*

273 Upstream, dissolved Cu concentrations range from ~17 mg/L to ~120 mg/L and
274 insignificant differences have been detected between concentrations in the < 0.22 μm fraction
275 and in the < 1,000 Da fraction (see Table 1), revealing the absence of Cu in the colloidal
276 phase (1 kDa - 0.22 μm). Copper concentrations obtained during this campaign are in good
277 agreement with those measured previously in the Odiel watershed and its sub-watersheds

278 (e.g., Sanchez Espana et al., 2005; Sarmiento et al., 2009a,b; Grande et al., 2010; Moreno
279 Gonzalez et al., 2020). Dissolved Cu concentrations decrease to 0.29 - 1.65 mg/L in the
280 downstream point. In both sampling points, dissolved Cu is highly correlated with SO₄
281 (R²=0.99 between Cu and SO₄), Fe concentrations (Fig. 2 and 3) and other elements. To
282 illustrate the link between these elements, we reported the relationship obtained between Cu
283 and Ni concentrations for both upstream and downstream points (Figure SI-1). In order to
284 explore multiple correlations between parameters (time, concentrations...), a Partial Least
285 Square Analysis method was necessary since we have more variables than individuals (Wold,
286 1985; Abdi, 2010) (see Fig. SI-2). The inertia graph reveals that only one single factor is
287 interpretable (Fig. SI-2A). The two sites are clearly distinguished by their chemical
288 composition and by the evolution of concentrations through time (see Fig. SI-2C). In the
289 upstream point Cu and other element concentrations vary simultaneously as a function of time
290 (and water discharge variation) while concentrations are much more stable at the downstream
291 point.

292 Copper isotope compositions range from -0.47 to -0.08 ‰ (n = 9) and -0.63 to -0.31 (n = 7)
293 ‰ at upstream and downstream point, respectively (Table 1). These values are coherent but
294 more variable than those previously obtained in a similar context (-0.75 ± 0.13 ‰ in the Odiel
295 River, Borrok et al., 2008). Cu isotope composition of the Meca River suspended matter
296 collected on 12-May-2016 at 4:00 p.m. ($\delta^{65}\text{Cu}_{\text{suspended-matter}} = -0.41 \pm 0.03 \text{ ‰}$) is the same as
297 that of filtered water ($\delta^{65}\text{Cu}_{\text{Dissolved}} = -0.42 \pm 0.01 \text{ ‰}$, Table 2). On the contrary, the top layers
298 of bed sediments of the Meca River revealed more negative $\delta^{65}\text{Cu}_{\text{sediment}}$ of $-1.92 \pm 0.04 \text{ ‰}$.

299 Copper dissolved concentration and $\delta^{65}\text{Cu}$ values showed significant variation over a 24-h
300 period (Fig. 4). The upstream $\delta^{65}\text{Cu}$ values fluctuate between $-0.47 \pm 0.01 \text{ ‰}$ (2 σ) and $-0.08 \pm$
301 0.02 ‰ (2 σ). During high rainfall periods (high discharge regime), lower Cu concentrations
302 ($\approx 17 \text{ mg/L}$) and $\delta^{65}\text{Cu}$ values ($\approx -0.4 \text{ ‰}$) associated with higher pH (> 2.80) are observed.

303 During low water discharge period, we observe higher Cu concentrations (up to 120 mg/L),
304 lower pH (pH < 2.5) and higher $\delta^{65}\text{Cu}$ values (close to 0 ‰). In the downstream point, where
305 Cu concentrations are much lower, from 0.29 to 1.65 mg/L, the $\delta^{65}\text{Cu}$ is between -0.31 and -
306 0.63‰. Thus we observe similar tendency as in the upstream point with concomitant lower
307 $\delta^{65}\text{Cu}$ and Cu content.

308

309 *3.3. The suspended sediment of the Meca River: mineralogical characterization and chemical* 310 *analysis*

311 Two suspended matter samples from the Meca River upstream point (ME-A 11-May-2016
312 10:00 p.m.; ME-A 12-May-2016 4:00 p.m.) were studied using SEM-EDS and X-ray
313 diffraction while Raman spectroscopy has been performed on the ME-A 11-May-2016 10:00
314 p.m. sample.

315 The SEM observations of both samples revealed homogeneous composition of suspended
316 material. We note the predominance of a muscovite type mineral (see Fig. SI-3 supplementary
317 information) in both samples and the presence of quartz, Fe oxides, rutile (TiO_2) and grains
318 containing S + Fe + As + Pb or S + Fe + Pb or S + Fe associations. Based on results of the X-
319 ray diffraction (see Fig. SI-4), the mineral containing S + Fe + Pb + As appears to be a
320 beudantite type mineral, the mineral containing S + Fe is a copiapite type mineral and the
321 mineral containing S + Fe + Pb is a (plumbo)jarosite type mineral. Pyrite, Ti oxides, and Fe
322 oxides grains have been also observed in the ME-A 11-May-2016 10:00 p.m. sample. The
323 EDS system of the SEM did not allow detecting Cu in the investigated minerals. Raman
324 spectroscopy revealed the presence of Fe oxydes, Tioxydes, jarosite, plumbojarosite and
325 wavellite (hydrated aluminous phosphate) confirming the X-ray diffraction data (Fig. SI-5).

326 Collected sediments were mainly composed of Fe, Al, K and Pb (between 1 and 10%)
327 and contained Mg, Ti, As, Na, Zn, Sb and Cu as minor elements with concentrations between

328 0.1 and 1%. Due to our analytical protocol, Si and S were not analysed in the solids. All the
329 concentrations have been normalised to the upper crust composition (Taylor and McLennan,
330 1995) (see supplementary materials Fig. SI-6). Compare to the upper crust reference, the
331 suspended and bed load sediments are enriched in several elements in the order Sb >Pb>>>
332 Cu, Sn, Zn, Cd >> Co, Fe, Cr, V. Compare to the bed load sediment, the suspended sediments
333 present a significant enrichment in Cd >> Sn, Sb, Zn, Pb, > Co.

334

335 **4. Discussion**

336 *4.1. Discharge-related variations of Cu concentration and isotopic composition at upstream* 337 *sampling point of the Meca River*

338

339 During the rain-free period and steady-state conditions, the low water discharge (< 0.5 m³/s,
340 field measurement using the “bucket” method) is associated with low pH and high copper
341 (>100 mg/L) and other metals and sulphate concentrations in the dissolved phase (i.e., <0.22
342 µm) of the Meca River. An opposite tendency is observed during high rain and runoff. This
343 behavior is consistent with the streamflow - sulphate concentration relationship defined by
344 Galvan et al. (2009) (see chapter 2.2) and the fact that we observe in the present study a close
345 relationship between Cu and sulphate concentrations (see Fig. 2). The upstream δ⁶⁵Cu values
346 fluctuate significantly between -0.47 ‰ during high rainfall and -0.08 ‰ during low rainfall
347 (see Fig. 4). For the low water discharge period, we assume that the Meca River is mainly fed
348 by emptying lakes and galleries (groundwater) from the Tharsis mining district since the
349 upstream point is the integrative water collection point of the whole mining district (Perez-
350 Ostale, 2014). The close to zero values obtained during low water period therefore represent

351 the isotopic composition of water in direct contact with the sulfide-rich parent materials and
352 their host rocks.

353 The lower Cu concentrations (and other metals) obtained during the high water discharge
354 cannot be explained by a single dilution process by meteoric waters since Cu isotopic
355 composition drastically changed with time (Fig. 4). This implies that (an)other(s) source(s)
356 and/or process(s) contribute(s) to the flux of metals in the Meca River. We hypothesized that
357 the large amount of abandoned wastes ~~presents~~ within the Tharsis mining district of the Meca
358 River watershed could be a significant contributor during flood events. Indeed, Perez-Ostale
359 (2014) reported that more than 80 ha of wastes are present within the Tharsis mining district
360 without any remediation measures and thus represent a major source of elements (metals and
361 metalloids) during flood event. In the Lagunazo mine area (Iberian Pyrite Belt), negative
362 $\delta^{65}\text{Cu}$ value ($-0.70 \pm 0.04 \text{ ‰}$) has been reported for waters percolating through pyrite-rich
363 wastes (Viers et al., 2018). The Lagunazo mine, mined for copper, is constituted by a massive
364 sulfide deposit located North-West of the Tharsis deposit. If we consider this negative
365 signature as a first approximation of the average isotopic composition of waters percolating
366 through the abandoned wastes of the Tharsis mine plant, the leaching of waste during periods
367 of intense precipitation can induce a lower isotopic composition in the Meca River since this
368 river is the outlet of this mining area. In the event of rainfall and after prolonged dry period,
369 rain water quickly dissolves highly soluble sulphates or other secondary minerals that have
370 been deposited during the dry period within the wastes and in the major bed of the river
371 (Sanchez-Espana et al., 2005; Valente et al., 2013). The mineralogical study revealed the
372 presence of secondary minerals with characteristics of mine wastes (copiapite or jarosite type
373 minerals) but also the predominance of a muscovite type minerals suggesting also the
374 contribution of surrounding soils (see section 4.3).

375 We performed a mass-balance modelling to check if the isotopic composition of the Meca
376 River at the upstream point could be explained by a mixing of waters originating from these
377 two supposed main sources, lakes/galleries and leaching of abandoned wastes (Fig. 5). In this
378 modelling, the isotopic compositions of waters percolating through the wastes varied from -
379 0.45 to -1.95‰ with a Cu concentration set at 10 mg/L while the concentration and isotopic
380 composition of Cu in galleries and lakes were set at 150 mg/L and -0.05 ($\delta^{65}\text{Cu}$, in ‰),
381 respectively. The isotopic signature used to characterise the "waste" pool was chosen to
382 encompass the value obtained by Viers et al. (2018) (-0.70 ± 0.04 ‰) for waters percolating
383 through pyrite-rich wastes. Additional theoretical curve with $\delta^{65}\text{Cu}$ of -1.95‰ was required to
384 encompass the upstream points at intermediate concentrations of dissolved Cu (Fig. 5). It can
385 be seen that, while open mine lakes are the major source of riverine Cu during dry periods,
386 their role becomes minor during flood.

387 Another process that could interfere in the resulting isotopic composition of the Meca
388 River at the upstream point is precipitation of secondary minerals within the main stem.
389 Indeed, the upstream waters are slightly oversaturated with respect to jarosite
390 ($\text{KFe}_3(\text{SO}_4)_2(\text{OH})_6$), goethite (FeOOH), and a cupric ferrite type mineral (CuFe_2O_4) (see Fig.
391 6). It has been previously shown that goethite, jarosite and schwertmannite could precipitate
392 at the pH of 2 to 3 in the river water (Sanchez Espana et al., 2005). As the suspended matter
393 and bed load sediment were enriched in lighter isotopes ($\delta^{65}\text{Cu}_{\text{suspended-matter}} = -0.41 \pm 0.03$ ‰;
394 $\delta^{65}\text{Cu}_{\text{sediment}} = -1.92 \pm 0.04$ ‰), the minerals precipitation can exert strong effect on the
395 isotopic composition of the river water. For example, precipitation of isotopically-light solid
396 phases will enrich the river water in heavier isotopes via mass balance effect. Copper
397 exhibited heavier isotopic composition during low flow period but the effect cannot be
398 quantitatively assessed. However, the absence of copper in the form of small colloids (see
399 section 4.2) would suggest a source change rather than a process within the water column to

400 explain the variation in isotopic composition. Indeed, the precipitation of secondary minerals
401 should take place via precursors and in particular the presence of colloidal particles.

402 Overall, based on diel cycle under contrasting hydrological regime in the upstream point,
403 Cu isotopes allowed us to detect two distinct sources of Cu in the river, which are: *i*) lake
404 water under dry conditions, and *ii*) a mix of lake and soil/waste deposit runoff sources under
405 flood conditions. A multi-parametric statistical treatment suggests that the data structure is
406 governed by one single factor that could be related to the water discharge. With the exception
407 of Na and K, all elements exhibit a temporal pattern which is similar to that of Cu.

408
409 *4.2 Variations of Cu concentration and isotopic composition at the downstream sampling*
410 *point of the Meca River*

411
412 Located 20 km down from the upstream sampling point, the downstream point exhibits
413 much lower dissolved Cu concentrations (~0.28 mg/L to ~1.6 mg/L). With $\delta^{65}\text{Cu}$ values
414 ranging from $-0.63 \pm 0.03\text{‰}$ (2σ) to $-0.29 \pm 0.02\text{‰}$ (2σ), downstream sampling point exhibits
415 both narrower and negative values compared to upstream during the same sampling period
416 (Fig. 4A and 4B).

417 Because of the lack of hydrological data for both Meca River and tributaries it was impossible
418 for us to physically constrain the mixing processes. Consequently, we will discuss
419 qualitatively the processes that may affect the isotopic composition between the upstream and
420 the downstream points.

421 A dilution of mine waters by tributaries and lateral input through soils of the watershed are
422 primarily responsible for Cu isotope evolution over the Meca River watercourse. The lighter
423 isotopic composition of the downstream point could result from direct contribution of the
424 Meca tributaries through a dilution process. We sampled only one of these tributaries which

425 exhibited low Cu concentration (0.3 mg/L) and light isotopic composition ($\delta^{65}\text{Cu}_{\text{tributary}} = -$
426 $2.72 \pm 0.03 \text{ ‰}$). As this Meca tributary is draining non mining plant zone, we suggest our
427 sampling to be representative of the soil catchment contribution between the mine district and
428 the downstream sampling point. A small fraction of this Cu could be natural Cu originating
429 from the chemical weathering of the parental rocks that have an average value of 55 mg/kg
430 (Chopin and Alloway, 2007). A more significant fraction of Cu present in the surrounding
431 soils may originate from the mine after deposition of atmospheric particles on these soils.
432 Indeed, smelting activity was conducted on the Tharsis site for many years (Valente et al.,
433 2013) and Chopin and Alloway (2007) have revealed that in the case of Tharsis, the soils
434 appear to be contaminated significantly in the vicinity of the mine (2 to 3 km around). As
435 copper presents a strong affinity for organic matter, organic (O) soil horizons are generally
436 enriched in copper with respect to deepest soil horizons (Bigalke et al., 2011), what was
437 observed by Chopin and Alloway (2007). Based on a mass balance calculation,

$$438 \quad (\delta^{65}\text{Cu} \times [\text{Cu}])_{\text{downstream}} = (\delta^{65}\text{Cu} \times [\text{Cu}])_{\text{tribute_stream}} + (\delta^{65}\text{Cu} \times [\text{Cu}])_{\text{upstream}}$$

439 where [Cu] stands for Cu concentration, we estimated that 87 % of the downstream Cu comes
440 from the upstream point, and only 13% from the tributary streams.

441 In this case, it seems that only inputs of tributaries with exogenous Cu would be able to
442 affect $\delta^{65}\text{Cu}$ downstream values.

443 Furthermore, during the water flow between the mine/upstream and downstream point,
444 various in-stream processes could control Cu concentration and isotopic composition in the
445 fluid. These are: i) precipitations of secondary Cu-bearing minerals; ii) Cu sorption onto
446 major mineral phases of river bed sediments; iii) Cu uptake by aquatic microorganisms. These
447 processes are likely to be mostly pronounced in the downstream point, given that highly
448 acidic upstream waters (pH = 2.4 to 2.8) are not favourable for adsorption and biota

449 development. At the downstream point, speciation calculations show that the fluid is largely
450 oversaturated with respect to schwertmannite ($\text{Fe}_8\text{O}_8(\text{SO}_4)_x(\text{OH})_y, n\text{H}_2\text{O}$), a cuprite type
451 mineral (CuFe_2O_4) and at a lesser extent jarosite ($\text{KFe}_3(\text{SO}_4)_2(\text{OH})_6$), goethite (FeOOH) and
452 ferrihydrite ($\text{Fe}_2\text{O}_3, 0.5\text{H}_2\text{O}$) (see Fig. 6). Within the AMD context, it is known that the
453 heavier Cu isotopic composition of the solution with respect to that of bulk chalcopyrite could
454 be due to the precipitation of an isotopically light Cu-rich solid phase (Kimball et al., 2009).
455 More recent work suggested that the progressive enrichment of Cu heavier isotope along the
456 Cobica River, draining the Lagunazo copper mine, could be due to the precipitation of some
457 secondary minerals enriched in light isotopes (Viers et al., 2018). The values obtained for
458 suspended and bed sediments of the Meca River ($\delta^{65}\text{Cu}_{\text{susp-sed}} = -0.41 \pm 0.03 \text{‰}$ and
459 $\delta^{65}\text{Cu}_{\text{sediment}} = -1.92 \pm 0.04 \text{‰}$) seem to support this assumption since the secondary products
460 are enriched in light isotopes. However, given that the isotopic composition at the
461 downstream point (-0.29 to -0.63‰) is globally lower than that at the upstream point (-0.08
462 to -0.47‰), we suggest that secondary mineral precipitation cannot be sole process controlling
463 Cu isotope fractionation, and other mechanisms should be considered.

464 The higher pH measured at the downstream point (3.61 to 5.68) compared to the upstream
465 point (2.41 to 2.82) implies a possibility of metals sorption onto the surface of suspended
466 sediments in the course of the water flow, as it is known for other mine water-affected
467 environments (Lee et al., 2002; Smith, 1999). We identified the presence of Fe oxides and
468 other (hydr)oxide minerals in the suspended matter of the Meca River (see section 4.3) that
469 can offer substantial surfaces for Cu sorption. Balistreri et al. (2008) and Pokrovsky et al.
470 (2008) have shown that Cu sorption onto common mineral and organic surfaces favors the
471 heavy isotope leaving isotopically light Cu in the aqueous solution. The effect of the sorption
472 process could not be quantified but is consistent with a lower isotopic composition in the
473 downstream point.

474 Finally, third mechanism affecting Cu isotope composition in the river water is Cu
475 interaction with aquatic microorganisms. During our sampling period, the temperature was
476 low (13.6 – 17.1°C, upstream) and we did not detect any algal bloom that could have affected
477 the dissolved Cu. Moreover, the uptake of Cu by bacteria, periphytic biofilm or algae favors
478 the light Cu isotope into the biomass (Navarette et al. 2011; Coutaud et al., 2018). This
479 process would enrich the river water in heavy isotope, which is not consistent with our
480 observations.

481

482 ***5. Conclusions***

483 This study presented both Cu concentration and isotopic composition of the Meca River
484 draining one of the largest abandoned mine of the Iberian Pyrite Belt during a flood event.
485 Based on observations over the diel cycle under changing water regime conditions, Cu
486 isotopes are useful to understand the hydrochemical functioning of a complex mining zone. In
487 response to a change in the hydrological conditions, the system appears to react quickly since
488 Cu isotopic composition changes following the amount of precipitation/water discharge in the
489 mining area. In the case of the Tharsis mine, copper isotopes allowed us to detect two distinct
490 metal sources in the headwater catchment under constrained hydrological regime. A major
491 contribution was provided by lake/gallery source under dry conditions, whereas during the
492 flood, a mix of lake/gallery and soil/waste deposit contributed to lateral surface runoff. These
493 findings could be useful for mine remediation measures and monitoring practices. Twenty km
494 downstream the mine, the Cu isotopic composition is essentially controlled by a dilution and
495 mixing process of headwater catchment by lateral surface runoff within soils brought by
496 tributaries. It is not strongly modified by in-stream environmental processes such as

497 precipitation of Cu secondary bearing minerals, sorption on mineral surfaces or uptake by
498 aquatic organisms.

499

500

501 **Acknowledgments**

502 This work was supported by the EC2CO program of the INSU/CNRS institution and by the
503 European Union for co-funding SOIL TAKE CARE SOE1/P4/F0023 through the European
504 Regional Development Fund (ERDF), under the Interreg SUDOE Program. This work was
505 also partly supported by the EQUIPEX CRITEX programme (grant no. ANR-11-EQPX-0011,
506 Pls. J. Gaillardet and L. Longuevergne). We deeply thank Ludovic Menjot and Priscia Oliva
507 for their technical and scientific help in XRD data acquisition and interpretation, Manuel
508 Henry for his help in the clean room, and Stéphanie Mounic for anions concentrations
509 measurements at the GET laboratory. We want to also express our gratitude to our Stéphane
510 Le Blond du Plouy from the Centre de MicroCaractérisation Raimond Castaing for his
511 technical support in SEM-EDX characterisation. We would also like to thank the staff of the
512 management department without which nothing could be achieved. The reviewers should be
513 deeply thanked for their work.

514

515

516 **References:**

- 517 Abdi, H. 2010. Partial least squares regression and projection on latent structure regression (PLS
518 Regression). Wiley Interdisciplinary Reviews: Computational, <https://doi.org/10.1002/wics.51>
- 519 Achterberg E.P., Herzl V.M.C., Braungardt C.B., Millward G.E., 2003. Metal behaviour in an estuary
520 polluted by acid mine drainage: the role of particulate matter. *Environ. Pollut.* 121, 283-292.
- 521 Almodovar, G. R., Castro, J. A., Sobol, F., Toscano, M., 1997. Geology of the Riotinto Ore
522 Deposits, Geology and VMS deposits of the Iberian Pyrite Belt. SEG Fieldbook Series,
523 Society Economic Geologists, Volume 27, p. 165-172.
- 524 Balistrieri, L.S., Borrok, D.M., Wanty, R.B., Ridley, W.I., 2008. Fractionation of Cu and Zn isotopes
525 during adsorption onto amorphous Fe (III) oxyhydroxide: experimental mixing of acid rock
526 drainage and ambient river water. *Geochim. Cosmochim. Acta* 72(2), 311-328.
- 527 Bigalke, m., Weyer, S., Wilcke, W., 2011. Stable Cu isotope fractionation in soils during oxic
528 weathering and podzolization. *Geochim. Cosmochim. Acta* 75, 3119-3134.
- 529 Bigham, J.M., Schwertmann, U., Traina, S.J., Winland, R.L., Wolf, M., 1996. Schwertmannite and the
530 chemical modeling of iron in acid sulfate waters. *Geochim. et Cosmochim. Acta* 12, 2111-
531 2121.
- 532 Blondet I., Schreck E., Viers J., Casas S., Jubany I., Bahi N., Zouiten C., Dufrécho G., Freydier R.,
533 Galy-Lacaux C., Martinez-Martinez S., Faz A., Soriano-Disla M., Acosta J.A., Darrozes J.,
534 2019. Atmospheric dust characterisation in the mining district of Cartagena-La Unión, Spain:
535 Air quality and health risks assessment. *Sci. Tot. Environ.* 693, 133496.

- 536 Blotevogel S., Oliva P., Sobanska S., Viers J., Vezin H., Audry S., Prunier J., Darrozes J., Orgogozo
537 L., Courjault-Radé P., Schreck E., 2018. The fate of Cu pesticides in vineyard soils: A case
538 study using $\delta^{65}\text{Cu}$ isotope ratios and EPR analysis. *Chem. Geol.* 477, 35-46.
- 539 Borrok, D.M., Nimick, D.A., Wanty, R.B., Ridley, W.I., 2008. Isotopic variations of dissolved copper
540 and zinc in stream waters affected by historical mining. *Geochim. Cosmochim. Acta* 72(2),
541 329-344.
- 542 Chopin, E., Alloway, B., 2007. Distribution and mobility of trace elements in soils and vegetation
543 around the mining and smelting areas of Tharsis, Riotinto and Huelva, Iberian Pyrite Belt, SW
544 Spain. *Water, Air, and Soil Pollut.*, 182(1-4), 245-261.
- 545 Conde, C., Tornos, F., Large, R., Danyushevsky, L., Solomon, M., 2009. Análisis de elementos traza
546 por la LA-ICPMS en pirita de los sulfuros masivos de Tharsis (FPI). *Macla*, 63-64.
- 547 Coutaud M., Meheut M., Glatzel P., Pokrovski G.S., Viers J., Rols J-L., Pokrovsky O.S., 2018. Small
548 changes in Cu redox state and speciation generate large isotope fractionation during
549 adsorption and incorporation of Cu by a phototrophic biofilm. *Geochim. Cosmochim. Acta*
550 220, 1-18.
- 551 Dótor-Almazán, A., Armienta-Hernández, M.A., Talavera-Mendoza, O., Ruiz, J., 2017. Geochemical
552 behavior of Cu and sulfur isotopes in the tropical mining region of Taxco, Guerrero (southern
553 Mexico). *Chem. Geol.*, 471, 1-12.
- 554 Dupré B., Viers J., Dandurand J-L., Polvé M., Bénézech P., Vervier P., Braun J-J., 1999. Major and
555 trace elements associated with colloids in organic-rich river waters: Ultrafiltration of natural
556 and spiked solutions. *Chem. Geol.* 160, 63-80.
- 557 Elbaz-Poulichet, F., Braungardt, C., Achterberg, E., Morley, N., Cossa, D., Beckers, J., Nomérange,
558 P., Cruzado, A., Leblanc, M., 2001. Metal biogeochemistry in the Tinto–Odiel Rivers
559 (Southern Spain) and in the Gulf of Cadiz: a synthesis of the results of TOROS project. *Cont.*
560 *Shelf Res.* 21 (18–19), 1961–1973.
- 561 Fernandez, A., Borrok, D.M., 2009. Fractionation of Cu, Fe, and Zn isotopes during the oxidative
562 weathering of sulfide-rich rocks. *Chem. Geol.*, 264(1-4), 1-12.
- 563 Galvan L., Olias M., Fernandez de Villaran R., Domingo Santos J-M., Nieto J-M., Sarmiento A-M.,
564 Canovas C.R., 2009. Application of the SWAT model to an AMD-affected River (Meca River,
565 SW Spain). Estimation of transported pollutant load. *J. Hydrol.* 377, 445-454.
- 566 Grande J-A., de la Torre M-L., Céron J-C., Beltran R., Gomez T., 2010. Overall hydrochemical
567 characterization of the Iberian Pyrite Belt. Main acid mine drainage-generating sources
568 (Huelva, Spain). *J. Hydrol.* 390, 123-130.
- 569 Grande, J.A., Santisteban, M., De la Torre, M., Valente, T., Pérez-Ostale, E., 2013. Characterisation of
570 AMD pollution in the reservoirs of the Iberian Pyrite Belt. *Mine Water Environ.* 32(4), 321-
571 330.
- 572 Grande, J-A., Santisteban M., de la Torre, M.L., Davila, J.M., Perez-Ostale E., 2018. Map of impact
573 by acid mine drainage in the river network of The Iberian Pyrite Belt (Sw Spain).
574 *Chemosphere* 199, 269-277.
- 575 Kimball, B.E., Mathur, R., Dohnalkova, A.C., Wall, A.J., Runkel, R.L., Brantley, S.L., 2009. Copper
576 isotope fractionation in acid mine drainage. *Geochim. et Cosmochim. Acta* 73, 1247-1263.
- 577 Leblanc, M., Morales, J., Borrego, J., Elbaz-Poulichet, F., 2000. 4,500-year-old mining pollution in
578 southwestern Spain: long-term implications for modern mining pollution. *Econ. Geol.* 95(3),
579 655-662.
- 580 Lee, G., Bigham, J.M., Faure, G., 2002. Removal of trace metals by coprecipitation with Fe, Al and
581 Mn from natural waters contaminated with acid mine drainage in the Ducktown Mining
582 District, Tennessee. *Appl. Geochem.* 17(5), 569-581.
- 583 Marechal, C. N., P. Telouk, Albarède F., 1999. Precise analysis of copper and zinc isotopic
584 compositions by plasma-source mass spectrometry. *Chemical Geology* 156(1-4): 251-
585 273.
- 586 Mathur, R., Ruiz, J., Titley, S., Liermann, L., Buss, H., Brantley, S., 2005. Cu isotopic fractionation in
587 the supergene environment with and without bacteria. *Geochim. Cosmochim. Acta* 69(22),
588 5233-5246.

589 Mathur, R., Titley, S., Barra, F., Brantley, S., Wilson, M., Phillips, A., Munizaga, F., Maksaev, V.,
590 Vervoort, J., Hart, G., 2009. Exploration potential of Cu isotope fractionation in porphyry
591 copper deposits. *J. Geochem. Explor.* 102, 1-6.

592 Mathur, R., Munk, L.A., Townley, B., Gou, K.Y., Gomez Miguelez, N., Titley, S., Chen, G.G., Song,
593 S., Reich, M., Tornos, F., Ruiz, J., 2014. Tracing low-temperature aqueous metal migration in
594 mineralized watersheds with Cu isotope fractionation. *Appl. Geochem.* 51, 109-115.

595 Moreno-Gonzalez R., Canovas C.R., Olias M., Macias F., 2020. Seasonal variability of extremely
596 metal rich acid mine drainages from the Tharsis mine (SW Spain). *Environ. Pollut.* 259,
597 113829.

598 Navarrete, J.U., Borrok, D.M., Viveros, M., Ellzey, J.T., 2011. Copper isotope fractionation during
599 surface adsorption and intracellular incorporation by bacteria. *Geochim. Cosmochim. Acta* 75,
600 784-799.

601 Nieto, J.M., Sarmiento, A.M., Olias, M., Canovas, C.R., Riba, I., Kalman, J., Delvalls, T.A., 2007.
602 Acid mine drainage pollution in the Tinto and Odiel rivers (Iberian Pyrite Belt, SW Spain) and
603 bioavailability of the transported metals to the Huelva Estuary. *Environ. Int.* 33(4), 445-455.

604 Nimick, D.A., Gammons, C.H., Parker, S.R., 2011. Diel biogeochemical processes and their effect on
605 the aqueous chemistry of streams: A review. *Chem. Geol.* 283, 3-17.

606 Olias M., Canovas C.R., Basallote M.D., Macias F., Perez-Lopez R., Moreno-Gonzalez R., Millan-
607 Becerro R., Nieto J.M., 2019. Causes and impacts of a mine water spill from an acidic pit lake
608 (Iberian Pyrite Belt). *Environ. Pollut.* 250, 127-136.

609 Pérez Ostalé, E., 2014. Caracterización ambiental de estructuras mineras en la Faja Pirítica Ibérica
610 como soporte metodológico de gestión territorial. Tesis doctoral, Universidad de Huelva,
611 Spain.

612 Perez Rodriguez, N., Engström, E., Rodushkin, I., Nason, P., Alakangas, L., Öhlander, B., 2013.
613 Copper and iron isotope fractionation in mine tailings at the Laver and Kristineberg mines,
614 northern Sweden. *Appl. Geochem.* 32, 204-215.

615 Petit, J. C. J., de Jong, J., Chou, L., Mattielli, N. (2008). Development of Cu and Zn Isotope
616 MC-ICP-MS Measurements: Application to Suspended Particulate Matter and
617 Sediments from the Scheldt Estuary. *Geostandards and Geoanalytical Research* 32(2),
618 149-166.

619 Pokrovsky O., Viers J., Emnova E.E., Kompantseva E.I., Freyrier R., 2008. Copper isotope
620 fractionation during its interaction with soil and aquatic microorganisms and metal
621 oxy(hydr)oxides: possible structural control. *Geochim. et Cosmochim. Acta* 72, 1742-1757.

622 Roebbert, Y., Rabe, K., Lazarov, M., Schuth, S., Schippers, A., Dold, B., Weyer, S., 2018.
623 Fractionation of Fe and Cu isotopes in acid mine tailings: Modification and application of s
624 sequential extraction method. *Chem. Geol.* 493, 67-79.

625 Sáez R., Pascual E, Toscazo M. y Almodovar G. R., 1999. The Iberian type of volcanosedimentary
626 massive sulphide deposits. *Miner. Depos.* 34, 549-570.

627 Sainz, A., Grande, J., De la Torre, M., 2004. Characterisation of heavy metal discharge into the Ria of
628 Huelva. *Environ. Int.* 30(4), 557-566.

629 Sanchez Espana J., Lopez Pamo E., Santofimia Pastor E., Reyes Andrés J., Martin Rubi J-A., 2005.
630 The natural attenuation of two acidic effluents in Tharsis and La Zarza-Perrunal mines
631 (Iberian Pyrite Belt, Huelva, Spain). *Environ. Geol.* 49, 253-266.

632 Sanchez-Espana J., Yusta I., Diez-Ercilla M., 2011. Schwertmannite and hydrobasaluminite : A re-
633 evaluation of their solubility and control on the iron and aluminium concentration in acidic pit
634 lakes. *Appl. Geochem.* 26, 1752-1774.

635 Santisteban Fernandez M. (2015). Incidencia de procesos AMD en la hidroquímica de embalses
636 afectados en la faja pirítica ibérica. Thesis, Universidad de Huelva.

637 Sarmiento A.M., Nieto, J.M., Olias, M., Canovas, C.R., 2009a. Hydrochemical characteristics and
638 seasonal influence on the pollution by acid mine drainage in the Odiel River basin (SW Spain).
639 *Appl. Geochem.* 24, 697-714.

640 Sarmiento, A.M., Olias, M., Nieto, J.M., Canovas, C.R., Delgado J., 2009b. Natural attenuation
641 processes in two water reservoirs receiving acid mine drainage. *Sci. Total Environ.* 407, 2051-
642 2062.

- 643 Smith, K.S., 1999. Metal sorption on mineral surfaces: an overview with examples relating to mineral
644 deposits. *The environmental geochemistry of mineral deposits*. *Rev. Eco. Geol.* 6, 161-182.
- 645 Song, S., Mathur, R., Ruiz, J., Chen, D., Allin, N., Guo, K., & Kang, W., 2016. Fingerprinting two
646 metal contaminants in streams with Cu isotopes near the Dexing Mine, China. *Sci. Total*
647 *Environ.* 544, 677-685.
- 648 Teng, F.-Z., Dauphas, N., Watkins, J.M., 2017. Non-traditional stable isotopes: retrospective and
649 prospective. *Rev. Mineral. Geochem.* 82(1): 1-26.
- 650 Taylor, S.R., MacLennan, S.M. 1985. *The Continental Crust: its Composition and Evolution*.
651 Blackwell, Oxford (312 pp.).
- 652 Tornos, F., Solomon, M., Conde, C., Spiro, B., 2008. Formation of the Tharsis massive sulfide
653 deposit, Iberian Pyrite Belt: geological, litho-geochemical, and stable isotope evidence for
654 deposition in a brine pool. *Econ. Geol.* 103, 185–214.
- 655 Valente, T., Grande, J., De La Torre, M., Santisteban, M., Cerón, J., 2013. Mineralogy and
656 environmental relevance of AMD-precipitates from the Tharsis mines, Iberian Pyrite Belt
657 (SW, Spain). *Appl. Geochem.* 39, 11-25.
- 658 Vasyukova E.V., Pokrovsky O.S., Viers J., Oliva P., Dupré B., Martin F., Candaudap F., 2010. Trace
659 elements in organic- and iron-rich surficial fluids of the boreal zone : Assessing colloidal
660 forms via dialysis and ultrafiltration. *Geochim. et Cosmochim. Acta* 74(2), 449-468.
- 661 Viers J., Dupré B., Polvé M., Schott J., Dandurand J-L., Braun J-J., 1997. Chemical weathering in the
662 drainage basin of a tropical watershed (Nsimi-Zoétéélé site, Cameroon): comparison between
663 organic-poor and organic rich waters. *Chem. Geol.* 140, 181-206.
- 664 Viers, J., Grande, J.A., Zouiten, C., Freydier R., Masbou, J., Valente, T., de la Torre M-L.,
665 Destigneville, C., Pokrovsky, O.S., 2018. Are Cu isotopes a useful tool to trace metal sources
666 and processes in acid mine drainage (AMD) context? *Chemosphere*, 193, 1071-1079.
- 667 Viollier E., Inglett P.W., Hunter K., Roychoudhury, Van Cappellen P., 2000. The ferrozine method
668 revisited : Fe(II)/Fe(III) determination in natural waters. *Appl. Geochem.* 15, 785-790.
- 669 Wold, H. 1985. Partial Least Squares. In: Kotz, S. and Johnson, N.L., Eds., *Encyclopedia of Statistical*
670 *Sciences*, Vol. 6, John Wiley, New York, 581-591
- 671



Fig. 1: Upstream, tributary stream and downstream sampling locations within the Meca River. The Meca River is a tributary of the Odiel River (Huelva, Spain).

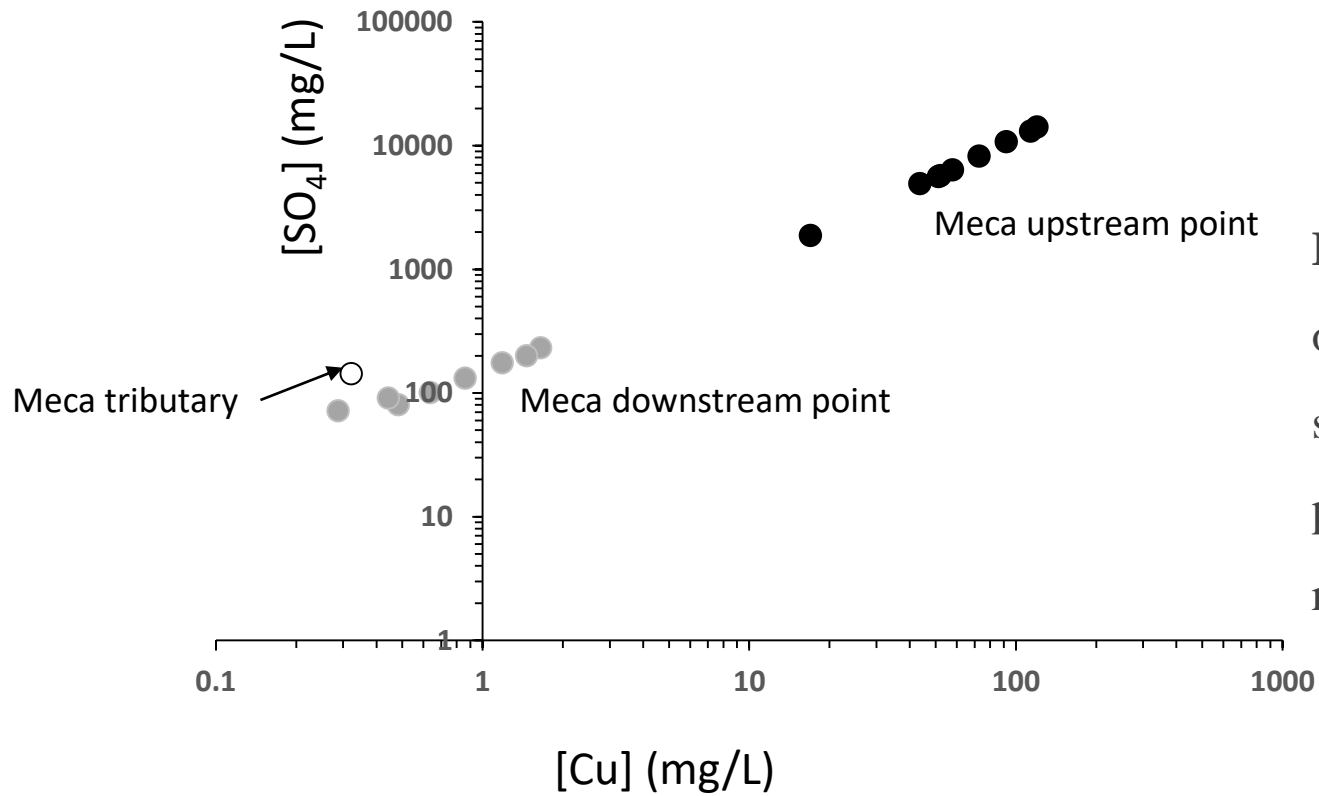


Figure 2: Dissolved Cu concentration as a function of SO_4^{2-} concentrations for upstream (black symbols) and downstream (gray symbols) sampling points of the Meca River. The Meca tributary is also reported.

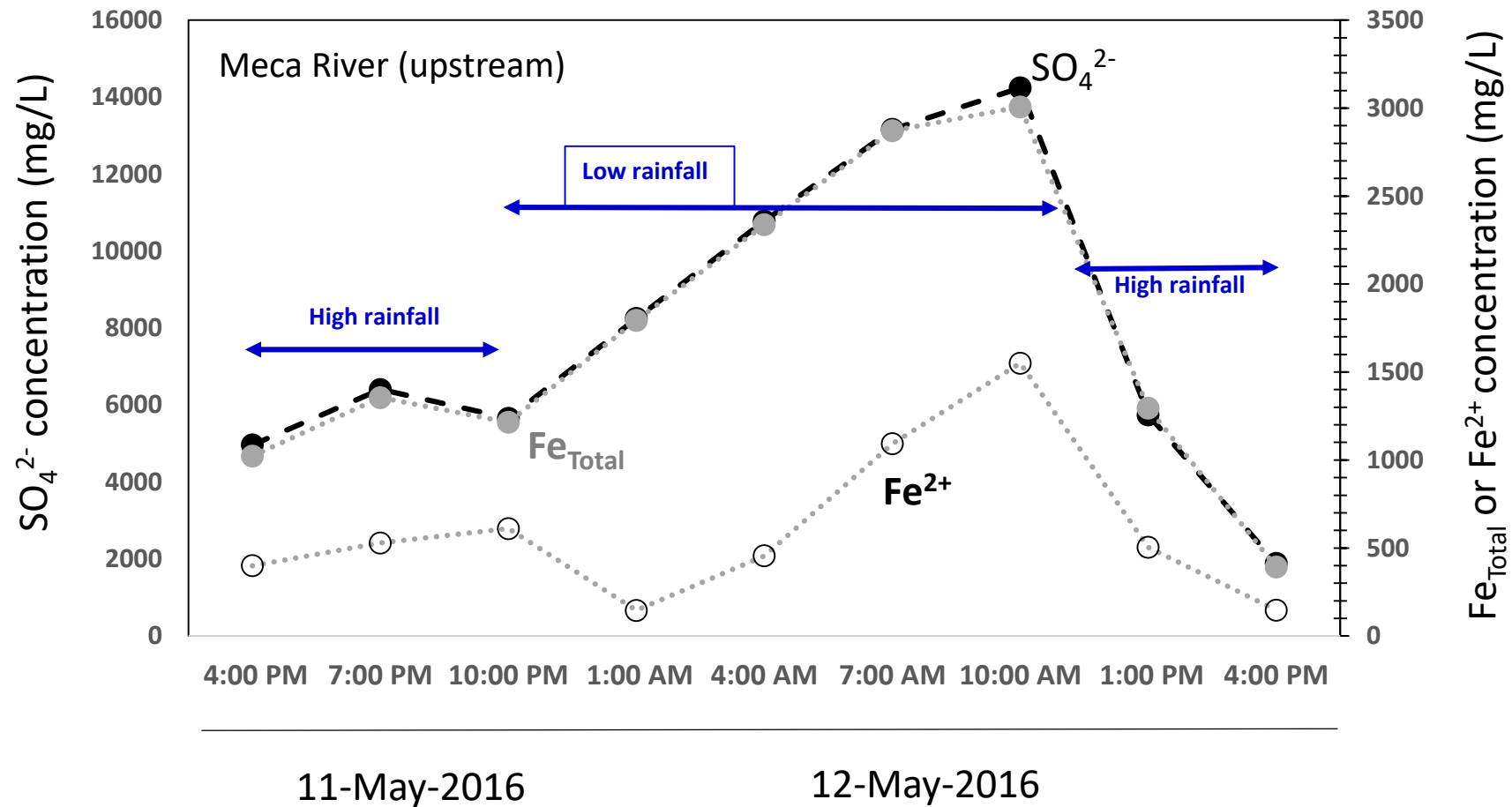


Figure 3: Dissolved SO₄²⁻ concentrations as a function of dissolved iron (Total and Fe²⁺) concentrations for upstream sampling points of the Meca River.

11-May-2016

12-May-2016

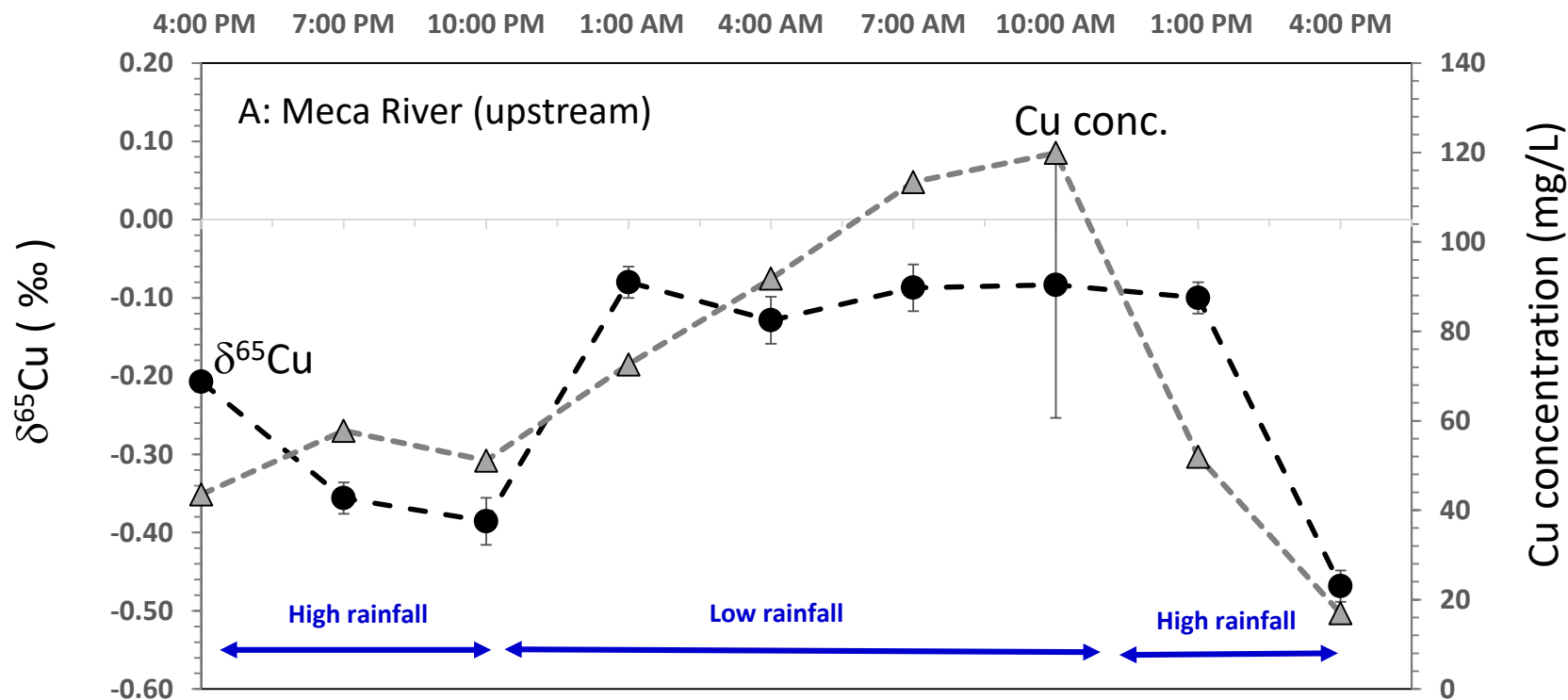


Figure 4: Diel variation in $\delta^{65}\text{Cu}$ (left axis, black circle) and dissolved Cu concentrations (right axis, gray triangle) for A) upstream and B) downstream. Error bars represent 2σ uncertainties calculated from replicate analyses.

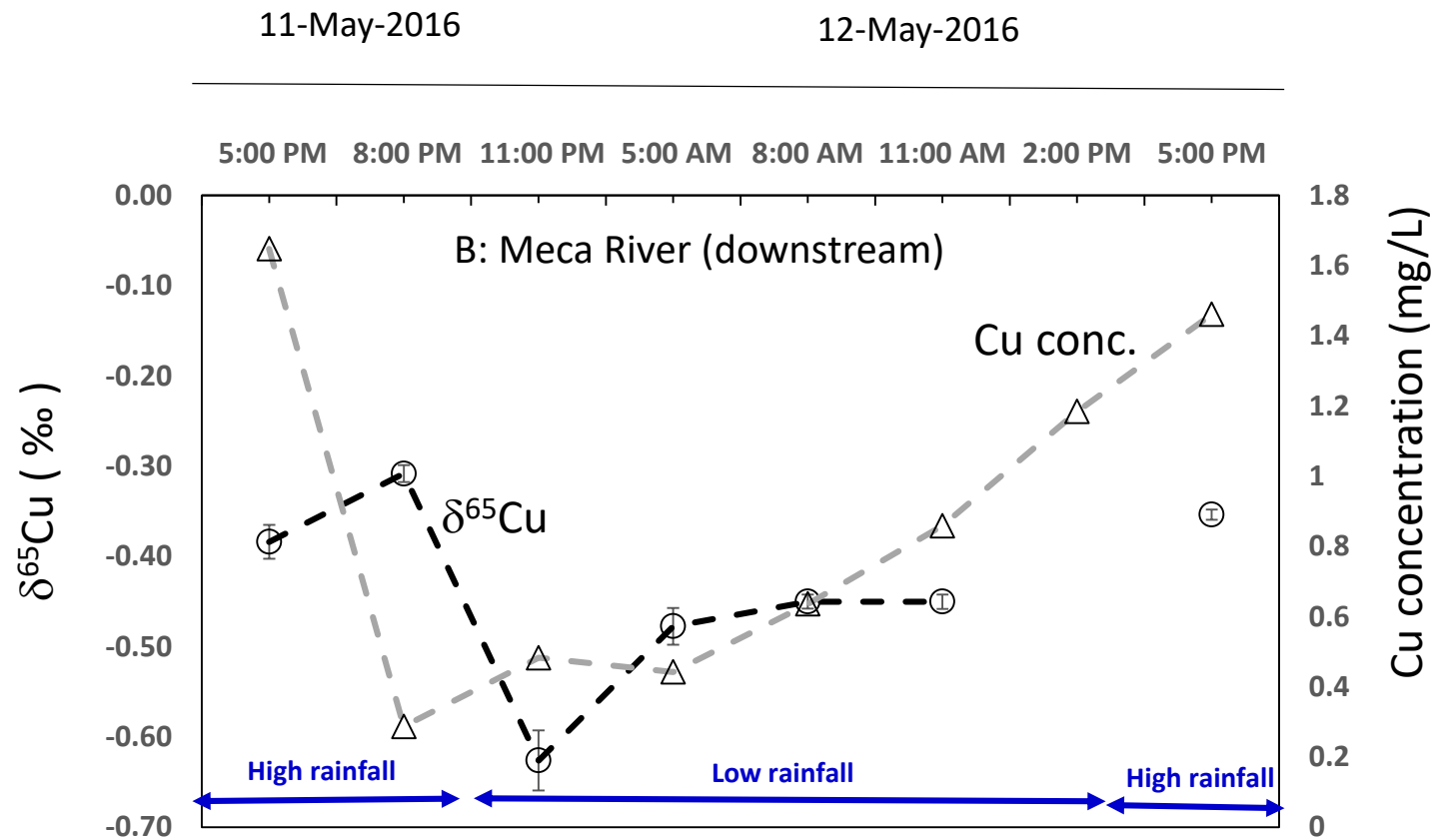


Figure 4 (to be continued)

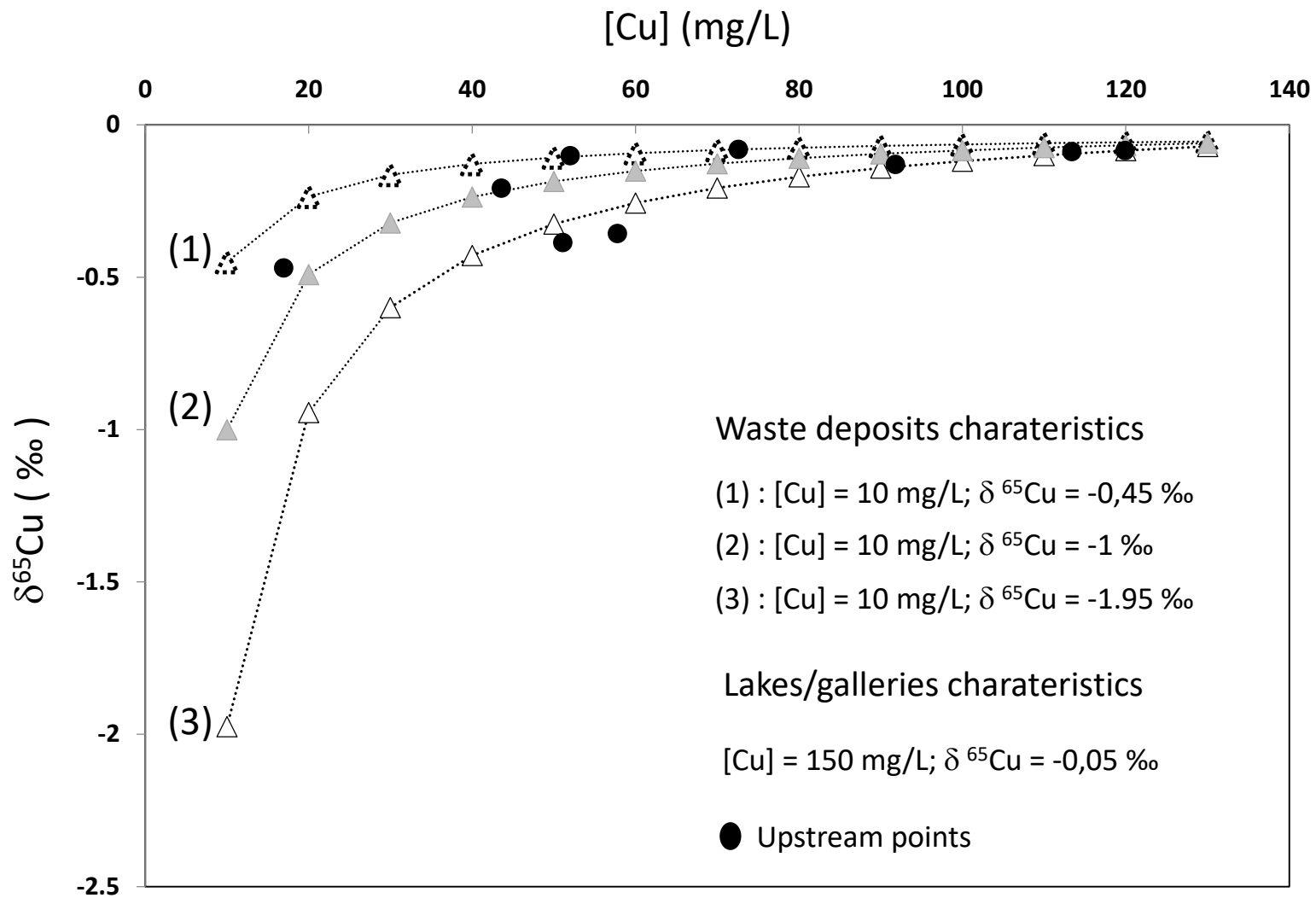


Figure 5: Theoretical mixing diagram between 1) water percolating through the wastes deposits and 2) water originating from the mine lakes and galleries. The black points are the values measured for the upstream sampling point.

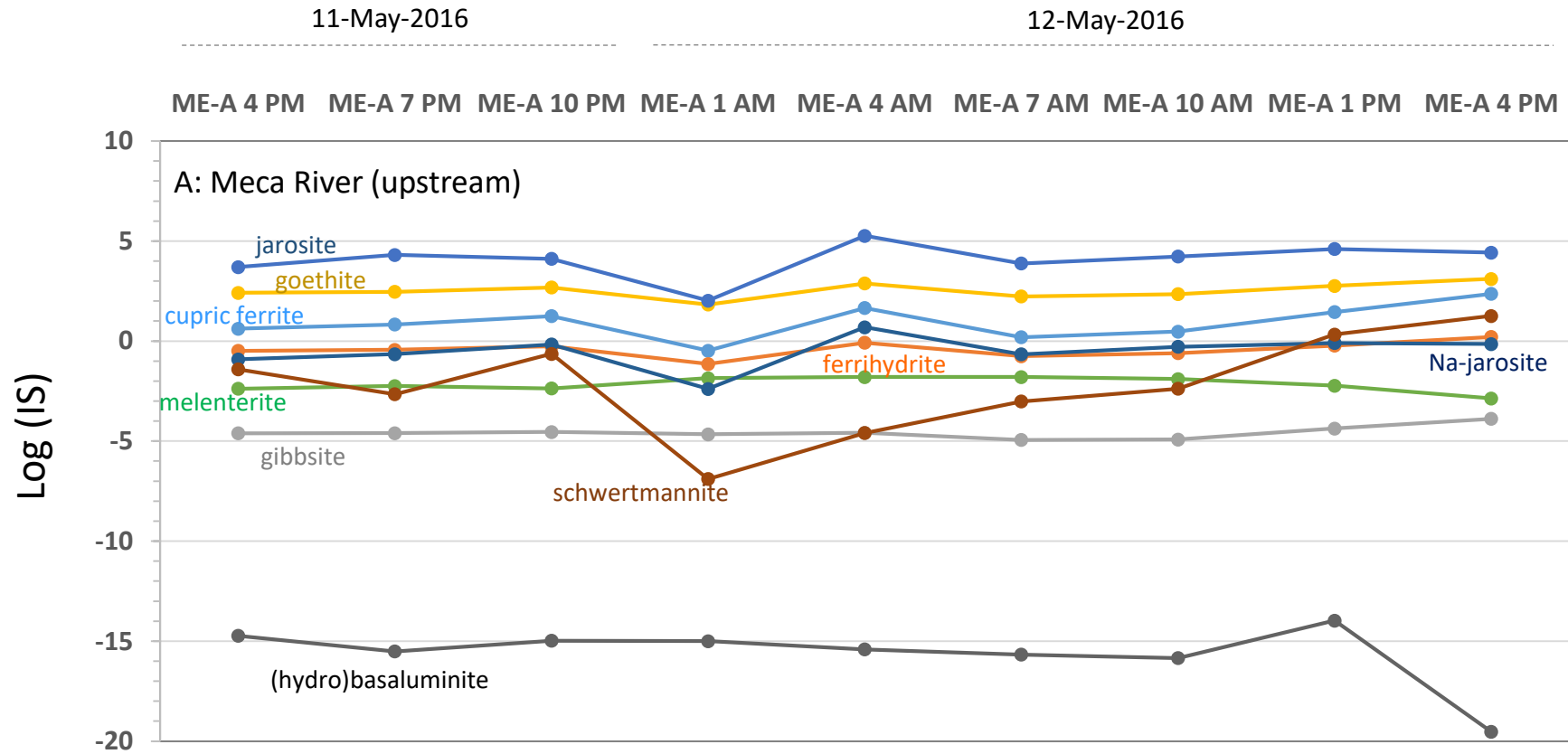


Figure 6: Saturation indexes calculated using Visual MINTEQ ver. 3.0. at both upstream and downstream sampling points of the Meca River.

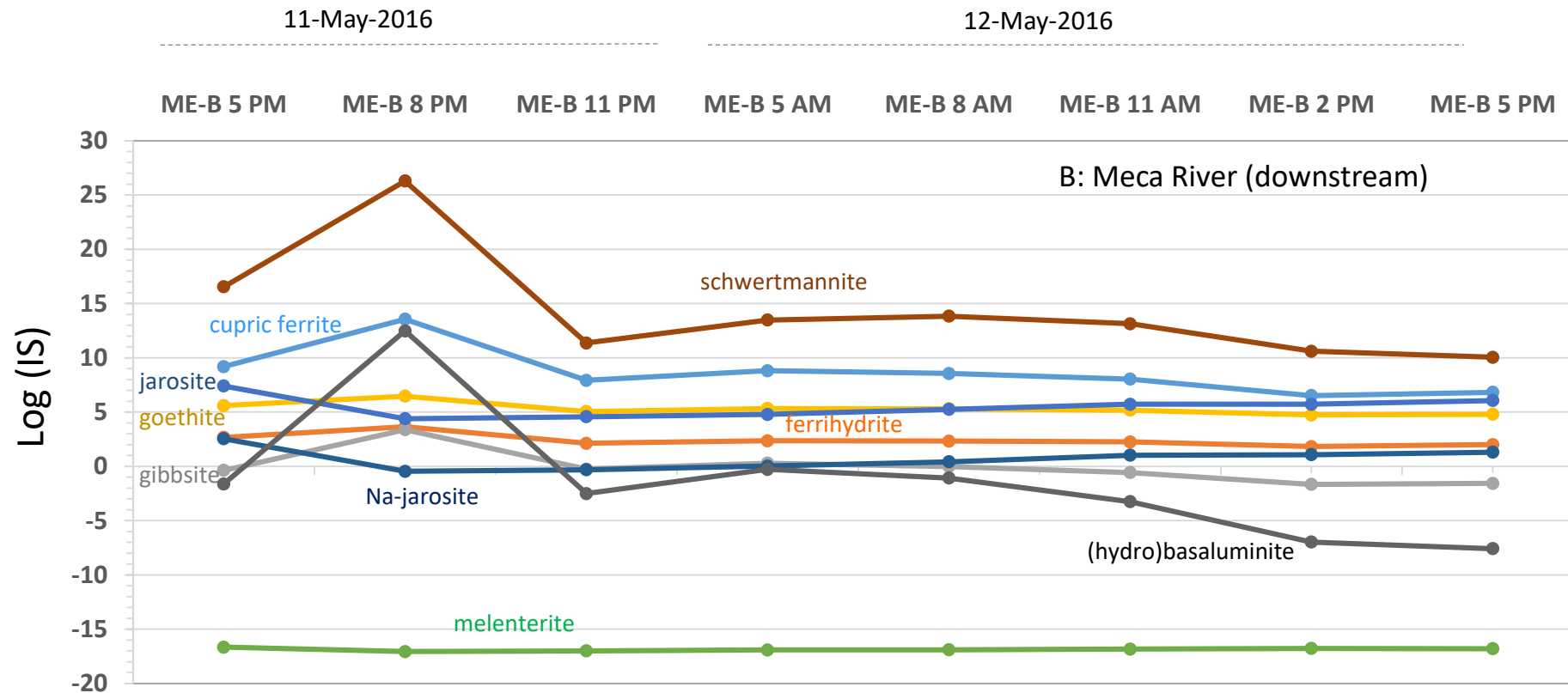


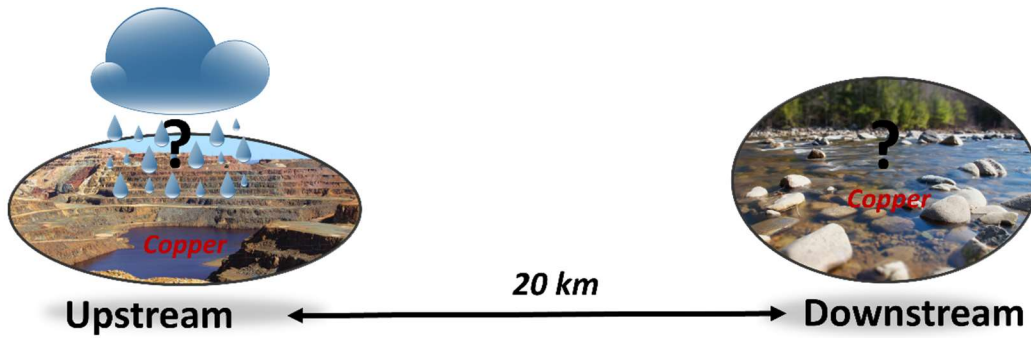
Figure 6: (to be continued)

Sampling date	11-May-2016 ME-A	11-May-2016 ME-A	11-May-2016 ME-A	11-May-2016 ME-A	11-May-2016 ME-A	12-May-2016 ME-A	12-May-2016 ME-A	12-May-2016 ME-A	12-May-2016 ME-A	12-May-2016 ME-A	12-May-2016 ME-A	12-May-2016 ME-A	12-May-2016 ME-A	11-May-2016 ME-A	11-May-2016 ME-B	11-May-2016 ME-B	11-May-2016 ME-B	12-May-2016 ME-B	12-May-2016 ME-B	12-May-2016 ME-B	12-May-2016 ME-B	12-May-2016 ME-B	
Sampling name	4:00 PM	4:00 PM	7:00 PM	10:00 PM	10:00 PM	1:00 AM	4:00 AM	4:00 AM	7:00 AM	10:00 AM	10:00 AM	1:00 PM	4:00 PM	ME-A	5:00 PM	8:00 PM	11:00 PM	5:00 AM	8:00 AM	11:00 AM	2:00 PM	5:00 PM	
Filtration size	<0,22 µm	<1000 da	<0,22 µm	<0,22 µm	<1000 da	<0,22 µm	<0,22 µm	<1000 Da	<0,22 µm	<0,22 µm	<1000 Da	<0,22 µm	<0,22 µm	<0,22 µm	<0,22 µm	<0,22 µm	<0,22 µm	<0,22 µm	<0,22 µm	<0,22 µm	<0,22 µm	<0,22 µm	<0,22 µm
Unit																							
Temperature (°C)	°C	16,6	-	17,1	15,4	-	14,3	14,3	-	13,8	15,0	-	13,6	17,0	15,7	16,6	19,7	16,2	14,4	14,4	15,6	16,7	21,0
pH		2,60	-	2,52	2,57	-	2,56	2,50	-	2,43	2,41	-	2,64	2,82	3,85	4,12	5,68	4,27	4,52	4,34	4,09	3,69	3,61
Conductivity	<i>mS/cm (at 25°C)</i>	5,48	-	6,44	6,12	-	8,02	9,76	-	11,39	11,6	-	6,22	2,81	0,51	0,43	0,31	0,31	0,31	0,38	0,39	0,54	0,50
O ₂	<i>mg/L</i>	6,46	-	6,30	6,61	-	6,64	6,45	-	6,54	6,48	-	8,4	7,65	6,94	-	-	-	-	-	-	-	-
DOC	<i>mg/L</i>	7,348	-	16,43	7,384	-	13,58	12,7	-	5,676	5,468	-	10,22	9,917	35,93	-	-	-	-	-	-	-	-
Cl	<i>mg/L</i>	10,67	-	11,61	11,12	-	11,98	12,85	-	13,80	14,07	-	8,85	8,28	21,84	25,03	29,11	26,29	30,19	26,89	26,76	27,69	17,32
NO ₃	<i>mg/L</i>	1,07	-	0,95	1,09	-	1,19	1,08	-	1,01	0,84	-	0,80	1,25	34,74	1,93	1,88	2,12	2,26	1,65	1,74	1,89	3,09
SO ₄	<i>mg/L</i>	4964	-	6407	5657	-	8251	10784	-	13163	14241	-	5746	1886	144	233	72	81	91	101	132	177	201
δ ⁶⁵ Cu (‰)		-0,21 (± 0,00)	-	-0,36 (± 0,02)	-0,39 (± 0,02)	-	-0,08 (± 0,03)	-0,13 (± 0,16)	-	-0,09 (± 0,02)	-0,08 (± 0,17)	-	-0,10 (± 0,02)	-0,47 (± 0,02)	-2,72 (± 0,03)	-0,38 (± 0,02)	-0,31 (± 0,01)	-0,63 (± 0,03)	-0,48 (± 0,02)	-0,45 (± 0,01)	-0,45 (± 0,01)	-	-0,35 (± 0,01)
Cu	<i>mg/L</i>	43,55	44,60	57,76	51,07	49,79	72,58	91,79	92,84	113,38	119,88	116,80	51,97	16,92	0,32	1,65	0,29	0,48	0,44	0,64	0,86	1,18	1,46
Na (mg/L)	<i>mg/L</i>	12,24	8,06	18,61	8,63	8,61	8,72	10,90	9,41	10,34	10,02	9,22	7,41	6,80	17,11	14,18	16,22	14,28	15,43	15,06	14,97	15,42	10,85
Mg (mg/L)	<i>mg/L</i>	267	256	334	282	283	419	530	549	672	723	693	313	91	16	17	10	9	10	11	12	14	14
Al (mg/L)	<i>mg/L</i>	298	283	358	317	319	468	602	628	775	826	799	360	101	3	12	1	3	2	4	6	8	10
Si (mg/L)	<i>mg/L</i>	16,04		20,12	18,12		22,56	25,06		27,63	29,33		14,33	8,54	5,29	4,95	4,12	4,03	4,31	4,77	-	5,19	5,51
K (mg/L)	<i>mg/L</i>	1,22	1,11	2,71	0,54	1,31	0,67	0,97	1,02	0,92	0,88	1,11	1,27	1,11	3,38	2,05	2,38	2,20	1,87	1,73	1,72	1,66	1,84
Ca (mg/L)	<i>mg/L</i>	54,10	47,81	100,17	54,25	51,10	70,70	85,65	86,89	106,17	112,66	108,95	50,72	19,05	21,92	10,49	9,81	8,56	8,96	8,90	9,34	10,04	9,48
Mn (mg/L)	<i>mg/L</i>	34,01	33,16	42,28	36,49	35,05	51,94	65,61	65,34	80,08	84,27	82,53	37,43	11,93	1,67	1,56	0,73	0,72	0,62	0,80	1,01	1,27	1,53
Fe (total)	<i>mg/L</i>	1023	1029	1355	1214	1157	1793	2337	2338	2872	3007	2924	1295	392	1	21	2	4	4	6	9	14	19
Fe ²⁺	<i>mg/L</i>	623	n.m.	826	604	n.m.	1648	1881	n.m.	1779	1456	n.m.	791	245	n.m.	n.m.	n.m.	n.m.	n.m.	n.m.	n.m.	n.m.	n.m.
Fe ³⁺	<i>mg/L</i>	400	n.m.	528	610	n.m.	145	456	n.m.	1093	1551	n.m.	504	147	n.m.	n.m.	n.m.	n.m.	n.m.	n.m.	n.m.	n.m.	n.m.
Co	<i>mg/L</i>	3,07	3,14	3,99	3,43	3,35	4,97	6,31	6,36	7,82	8,17	7,99	3,58	1,09	0,05	0,12	0,03	0,04	0,04	0,05	0,07	0,09	0,11
Ni	<i>mg/L</i>	1,06	1,10	1,39	1,16	1,15	1,71	2,16	2,19	2,70	2,88	2,81	1,23	0,39	0,02	0,05	0,02	0,02	0,02	0,02	0,02	0,03	0,04
Zn	<i>mg/L</i>	122,7	122,7	158,1	138,2	132,7	202,7	265,7	268,9	333,8	354,0	344,4	153,2	43,9	0,5	4,8	1,0	1,3	1,3	1,8	2,5	3,5	4,3
V	<i>µg/L</i>	220	225	290	270	255	388	512	519	629	649	629	272	87	0,33	0,10	0,06	0,05	0,07	0,05	0,04	0,04	0,05
Cr	<i>µg/L</i>	184	181	247	217	207	314	411	408	505	538	531	229	66	1,36	5,54	0,39	0,80	0,98	1,33	2,34	3,70	5,05
Cd	<i>µg/L</i>	264	254	328	280	272	422	543	551	682	734	719	315	88	0,66	10,77	2,63	3,20	2,97	4,21	5,65	7,75	9,49

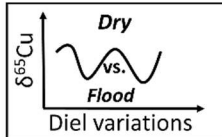
Table 1: Physical parameters (*measured in situ*), elemental concentrations and Cu isotopic composition for the upstream and downstream sampling points of the Meca River and for the Meca tributary. All concentrations and isotopic were measured in the dissolved fraction (i.e., <0.22 µm). n.m. indicates not measured.

Sampling date	11-May-2015	11-May-2015	12-May-2016	12-May-2016	12-May-2016
Sampling name	MES ME-A 4:00 PM	MES ME-A 10:00 PM	MES ME-A 4:00 AM	MES ME-A 4:00 PM	bed sediment ME-A
unit:	$\mu\text{g/g}$	$\mu\text{g/g}$	$\mu\text{g/g}$	$\mu\text{g/g}$	$\mu\text{g/g}$
$\delta^{65}\text{Cu}$ (‰)	-0,41 (\pm 0.03)	-	-	-	-1,92 (\pm 0.04)
Na	2507	2082	822	3575	10461
Mg	3434	4788	4071	3364	5144
Al	79220	68049	30526	102033	69998
K	18927	16826	4708	25216	19269
Ti	3037	3834	1160	3391	5024
V	115	102	46,7	146	126
Cr	86,1	82,7	43,0	96,5	85,6
Mn	278	439	478	214	275
Fe	112293	132229	66202	101090	129246
Co	38,2	55,2	50,4	20,7	15,6
Ni	27,3	25,8	22,5	28,7	34,9
Cu	669	909	788	479	392
Zn	1126	1554	1928	447	349
As	2831	2689	1653	1984	1009
Se	89	80	75	36	47
Rb	111	103	40	164	73
Sr	78,7	86,3	32,6	96,5	50,1
Y	12,5	15,9	6,8	15,5	19,3
Mo	7,68	8,73	4,15	4,73	3,96
Cd	2,23	3,45	4,00	0,80	0,36
Sn	235	91	185	46	54
Sb	1100	983	776	379	220
Cs	6,72	5,08	2,46	9,03	3,14
Ba	457	473	166	547	288
La	29,6	42,5	12,5	41,7	16,4
Ce	61,2	75,6	24,3	79,7	33,9
Pr	6,94	8,42	2,99	8,86	4,37
Nd	25,3	31,1	10,7	32,8	16,5
Sm	4,79	5,46	2,06	6,12	3,59
Eu	1,13	1,12	0,44	1,13	0,63
Tb	0,47	0,55	0,25	0,55	0,56
Gd	5,61	3,97	2,69	4,25	4,35
Dy	2,51	3,03	1,31	3,02	3,71
Ho	0,50	0,60	0,26	0,60	0,89
ER	1,63	1,97	0,85	1,97	2,71
Tm	0,25	0,31	0,14	0,31	0,43
Yb	1,92	2,25	0,90	2,22	3,03
Lu	0,31	0,36	0,13	0,36	0,45
Pb	7530	9466	4258	4320	1773
Th	10,0	14,9	3,9	16,0	12,1
U	3,45	3,95	1,75	3,13	4,15

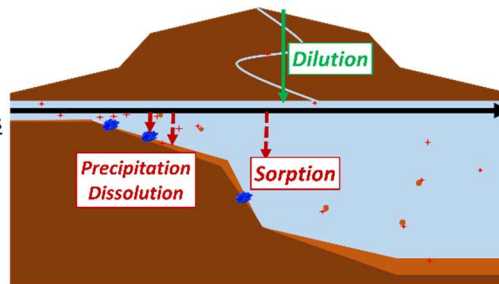
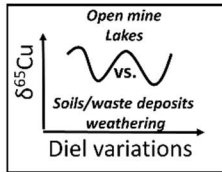
Table 2: Elemental concentrations and Cu isotopic composition for the suspended and bed sediments from the Meca River.



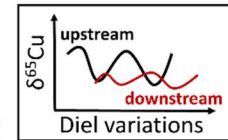
Copper isotopes vs. hydrology



Copper isotopes vs. sources



Copper isotopes response to upstream signal



- Detection of delayed upstream input
- Lower sensitivity
- Influence of tributary streams

Conservative processes

Non-conservative processes